Stability and Improvement of *LCL*-filtered Inverters Using Only Grid Current Feedback Active damping for Weak Grid Applications

Jinming Xu, Binfeng Zhang and Shaojun Xie
College of Automation Engineering
Nanjing University of Aeronautics and Astronautics
Nanjing, China
xjinming01@163.com

***Abstract*—For the grid-connected *LCL*-filtered inverter, for the purpose of using a minimal number of sensors, the grid current feedback active damping (GCFAD) based closed-loop control was widely discussed. However, the performance with such control was seriously affected by the grid conditions at the point of common coupling (PCC), especially the large grid impedance. Thus, in this study, the stability with GCFAD in the weak grid is discussed first and the relations between the robustness and system parameters are derived by mathematic derivations. The contradiction between the control bandwidth and the robustness is found. Based on the above analysis, a novel phase shaping method has been proposed for GCFAD to maintain a high robustness with a desired bandwidth. Selected simulation and experimental waveforms are provided to show the correctness of the analysis and the effectiveness of the improved control approach.**

Keywords—Inverter; LCL filter; grid impedance; grid current active damping; stability; robust control

I. INTRODUCTION

The grid-connected inverter with an *LCL* or *LCL*-Trap filter is the key interface in the distributed power generation systems [1]. Although the high-order filter can highly suppress the switching harmonics, the resonance of high-order filter has to be solved [2]. To solve the *LCL*-filter resonance, a lot of passive damping [3] and active damping (AD) methods (such as the capacitor current feedback AD) were proposed. Recently, many studies paid special attentions to the current control with only one current feedback for the sake of using as few sensors as possible, including the delay-dependent current control [4]-[5], the notch filter AD [6]-[9] and the grid current feedback AD (GCFAD) [10]-[13] and so on. Among them, the GCFAD can be adopted simply through high-pass filter (HPF) with an optimal design [10]. Besides, the studies in [12]-[13] analyzed the GCFAD stability while considering the digital control delay, and provided some useful recommendations in the applications.

In the practical applications, besides the voltage harmonics in the PCC voltage, the PCC grid can be very weak with non-negligible grid impedance [14]-[16]. However, the robustness of the GCFAD-based current control with only the grid current feedback in the weak grid case has not been deeply discussed. It is true that several robust or adaptive control methods were proposed by [17]-[21] recently, but these studies all used the capacitor current feedback AD (requiring extra sensors). The way to enhance the robustness of GCFAD remains unsolved.

In summary, recent studies aims at improving the inverter performance while reducing the number of sensors used. But the performance with the GCFAD (with only the grid current sensor) in the weak grid case has not been studied. Hence, this study aims to investigate and enhance the robust performance with the GCFAD in the weak grid case.

II. STRUCTURE AND MODELLING OF GRID CURRENT FEEDBACK ACTIVE DAMPING (GCFAD)

Fig. 1 shows the basic structure of a grid-connected LCL-filtered inverter, where the *LCL* filter consists of an inverter-side inductor L_1, a capacitor C_1, and a grid-side inductor L_2. Only the grid current i_g and the PCC voltage u_g are sampled for the control and phase-locked loop. i_{L1} is the inverter-side current, u_{inv} is the inverter output voltage. In the practical case, the dc-link U_{dc} can be the renewable source or a front DC-DC converter in the distributed power generation systems.

To solve the inherent resonance produced by the *LCL* filter, plenty of AD methods have been proposed. The study in [2]

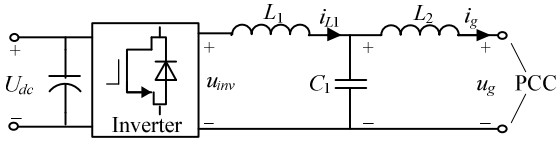

Fig. 1 Grid-connected *LCL*-filtered inverter

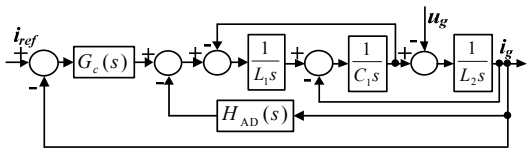

Fig. 2 Typical grid current feedback AD control structure

gives an overview of the existing resonance damping strategies and shows some comparative results. The GCFAD-based grid current control is shown in Fig. 2 where i_{ref} is the grid current reference, $G_c(s)$ is the current controller, $H_{AD}(s)$ is the grid current feedback AD function expressed as:

$$H_{\mathrm{AD}}(s) = -\frac{k_{\mathrm{AD}} s}{s+\omega_h} \tag{1}$$

where k_{AD} and ω_h are separately the proportional gain and the turnover frequency of the high-pass filter. Following [10], the AD parameters ω_h and k_{AD} are selected according to

$$\begin{cases} \omega_h = 2\omega_{res}\sqrt{1-k^2} \\ k_{\mathrm{AD}} = \omega_{res}(L_1+L_2)(2-k^2)\sqrt{1-k^2} \end{cases} \tag{2}$$

where k is a positive number which is recommended from 0.8 to 0.9 for a high bandwidth.

For the grid-connected inverter in the weak grid case, the impedance-based stability criterion is used to investigate the system robustness [14]. The inverter-grid system considering the grid impedance can be modeled in Fig. 3 [14] where i_c is the equivalent current source, Z_{out} is the inverter output impedance, Z_g is the grid impedance, and u_s is the grid voltage. Given that the inverter is stable without the grid impedance, the inverter-grid system is stable only if Z_g/Z_{out} satisfies the Nyquist criterion (by counting the number of ±180°-crossings only in the frequency range with gains above 0dB [6]).

The current-controlled inverter can be depicted in Fig. 4 where u_{inv} is a dependent voltage source related to the current control in Fig. 2, i.e., the expression of u_{inv} is:

$$u_{inv} = (i_{ref} - i_g)\cdot G_c(s) - i_g \cdot H_{\mathrm{AD}}(s) \tag{3}$$

Kirchhoff's laws tell:

$$\begin{cases} u_{inv} = L_1 s \cdot i_{L1} + L_2 s \cdot i_g + u_g \\ \dfrac{1}{C_1 s}\cdot(i_{L1} - i_g) = L_2 s \cdot i_g + u_g \end{cases} \tag{4}$$

Using (3) and (4), Z_{out} can be calculated as:

$$\begin{aligned} Z_{out} &= \left.\frac{u_g}{(-i_g)}\right|_{i_{ref}=0} \\ &= \frac{L_1L_2C_1s^3 + (L_1+L_2)s + H_{\mathrm{AD}}(s) + G_c(s)}{L_1C_1s^2+1} = \frac{N_{out}(s)}{D_{out}(s)} \end{aligned} \tag{5}$$

Then, Z_g/Z_{out} must satisfy the Nyquist criterion.

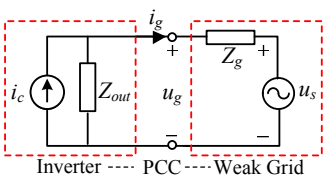

Fig. 3 Model of inverter-grid system considering the grid impedance

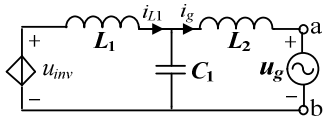

Fig. 4 Equivalent structure of current-controlled inverter

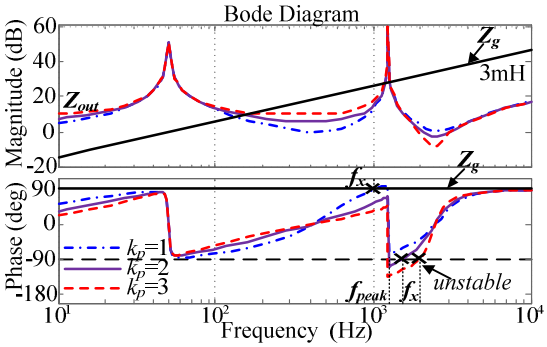

Fig. 5 Bode plots of Z_{out} with PR controller and Z_g

III. Problems of GCFAD in the Weak Grid Case

Using (5), Fig. 5 shows some Bode plots of Z_{out} with the variation of the proportional gain k_p of $G_c(s)$. The *LCL* parameters are L_1=0.755 mH, L_2=0.125 mH, C_1=22 μF with a switching frequency of 15 kHz and a rated power of 5 kW. For a short circuit ratio (SCR) of 10, Z_g can be 3.08 mH. Basically, with k_p increasing, magnitudes of Z_{out} at low frequencies increase, and the region where $|Z_g|$ is higher than $|Z_{out}|$ (i.e., the gain of Z_g/Z_{out} is above 0dB) is narrowed. Besides, Z_{out} crosses 90° at the frequency f_x (i.e., 0°-crossing for Z_g/Z_{out}) with a small k_p, and Z_{out} crosses −90° (i.e., 180°-crossing for Z_g/Z_{out}) with a large k_p.. Last, Z_{out} in (5) has two conjugated poles so that the magnitude curve has a peak and the phase curve decreases sharply at f_{peak}, i.e.,

$$f_{peak} = \frac{\omega_{peak}}{2\pi} = \frac{1}{2\pi\sqrt{L_1C_1}} \tag{6}$$

In Fig. 5, the system is stable only when k_p is 1. A stable inverter-grid system with the GCFAD should not have the −90°-crossing around f_x. Note that Z_{out} crosses either 90° or −90° due to the −180° variation at f_{peak}. Therefore, the specific stability criterion of the GCFAD is $f_x<f_{peak}$. Note that Z_{out} at f_x ($f_x\neq f_{peak}$) is a purely imaginary number, i.e.,

$$\mathrm{Re}\{H_{\mathrm{AD}}(j\omega_x) + G_c(j\omega_x)\} = 0 \tag{7}$$

Given that $G_c(s)$ at high frequencies can be readily seen as a proportional factor k_p, substituting (1) into (7) yields:

$$\begin{aligned}&\mathrm{Re}\left\{-\frac{jk_{\mathrm{AD}}\omega_x}{j\omega_x+\omega_h}+k_p\right\}=0\Rightarrow-\frac{k_{\mathrm{AD}}\omega_x^2}{\omega_x^2+\omega_h^2}+k_p=0\\&\Rightarrow f_x=\frac{\omega_h}{2\pi}\sqrt{\frac{k_p}{k_{\mathrm{AD}}-k_p}}\end{aligned}\tag{8}$$

Substituting (8) into $f_x<f_{peak}$ leads to the robustness criterion of the GCFAD, i.e.,

$$k_p<k_{p\_limit}=\frac{\omega_{peak}^2}{\omega_{peak}^2+\omega_h^2}k_{\mathrm{AD}}\tag{9}$$

For a certain set of *LCL* parameters, the maximum k_{p_limit} for high robustness is then determined.

If k_p is designed to achieve a high bandwidth, the robustness can be poor because k_p cannot satisfy (9). Even in the case that the bandwidth is low (i.e., with a small k_p), if k_p is close to the boundary in (9), the stability margin is too small to assure a good robust performance. For instance, in Fig. 3, if k_p is 2 to realize a high bandwidth, (9) is not fulfilled; if k_p is 1, although the system can be stably in the weak grid case, the phase at f_{peak} is very close to −90° yielding insufficient phase margin. It is still challenging for the GCFAD to work well in the weak grid.

IV. Proposed Phase Shaping Compensator for GCFAD in the Weak Grid Case

In order to improve the GCFAD in the weak grid case, the phases around f_{peak} should be improved. Fig. 6 shows the proposed phase shaping scheme where $G_{ps}(s)$ is the phase shaping compensator. Z_{out} turns to be:

$$Z_{out\_ps}=\frac{L_1L_2C_1s^3+(L_1+L_2)s+H_{\mathrm{AD}}(s)+G_c(s)}{L_1C_1s^2+1+G_{ps}(s)}=\frac{N_{out}(s)}{D_{out\_ps}(s)}\tag{10}$$

D_{out_ps} around f_{peak} can be expressed as:

$$D_{out\_ps}=L_1C_1s^2+1+G_{ps}(s)\tag{11}$$

Therefore, in order to freely shape the phases around f_{peak}, the desired expression of $G_{ps}(s)$ is:

$$G_{ps}(s)=k_{ps}s\tag{12}$$

where k_{ps} is a positive proportional factor.

With larger k_{ps}, the phases of Z_{out_ps} around f_{peak} can be improved much higher because of the increased damping factor

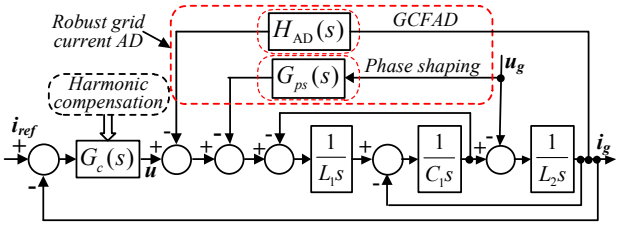

Fig. 6 Proposed phase shaping compensator for GCFAD

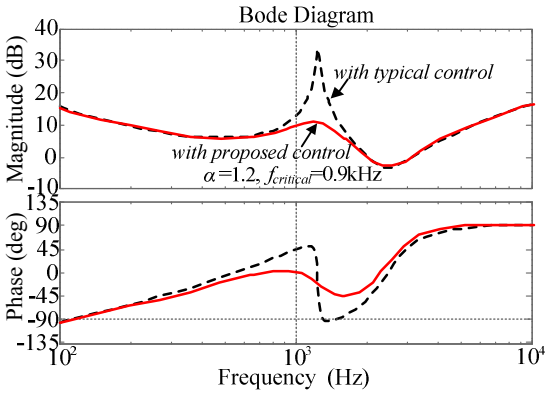

Fig. 7 Bode plot of Z_{out_ps} with the proposed control

of D_{out_ps}. But note that the side effect of using larger k_{ps} is that $G_{ps}(s)$ can affect the magnitudes of Z_{out_ps} at the frequencies below f_{peak}. Then, the lower-frequency impedance is affected and the rejection of the grid voltage-deduced current harmonics can be degraded. Therefore, the design of $G_{ps}(s)$ should ensure that it has negligible or slight impact on the low-frequency magnitudes of Z_{out_ps}. Given that N_{out} do not have relations with $G_{ps}(s)$, the design of $G_{ps}(s)$ is equivalent to the determination of the bandwidth of D_{out_ps} in (10). By defining $f_{critical}$ ($f_{critical}<f_{peak}$) as the critical frequency where the magnitude of Z_{out_ps} is expected to be not affected, the selection of k_{ps} should follow the criterion:

$$k_{ps}\le k_{ps\_critical}=\frac{1-L_1C_1(2\pi f_{critical})^2}{2\pi f_{critical}}\sqrt{\alpha^2-1}\tag{13}$$

where α indicates that the current harmonic at $f_{critical}$ with $G_{ps}(s)$ can be α multiplied by that without $G_{ps}(s)$. Readers can select the values of $f_{critical}$ and α according to the practical condition, given that $f_{critical}$ relates to the frequency band of major current harmonics and the selection of α should consider the limitation of current harmonics. For the case study, by selecting $f_{critical}$=1 kHz and α=1.2, here, Fig. 7 shows the Bode plot of Z_{out_ps}. The phase curve keeps a certain distance from −90° yielding a higher robustness.

Note that if *LCL* parameters were selected so that the value of k_p corresponding to a desirable bandwidth is much lower than the limited value in (9), the GCFAD can be robust even without the proposed phase shaping. Nevertheless, if the phase shaping is used in the above case, the robustness when the grid impedance varies can be further improved.

V. SIMULATIONS

In this section, performances with different strategies and different grid impedance values are tested, while the ac grid u_s contains some low-order voltage harmonics (i.e., 5% 3rd, 3% 5th~7th, and 2% 9th~13th). In the following sections, Strategy 1 denotes the grid current AD-based control and design in [10], while Strategy 2 represents the robust grid current control in this study.

Before the simulation, the current controller parameters are briefly explained. In the tests, f_b is always set at 1 kHz, which means that the gain of k_p is about 2. Generally, the harmonic resonant (HR) controller can be used to suppress the low-order grid current harmonics. The HR controller is expressed as:

$$G_{HR}(s) = k_p + k_r \sum_{n=1,3,5,\ldots}^{n_{\max}} \frac{s}{s^2 + \omega_c s + (n\omega_0)^2} \tag{14}$$

where ω_c represents the magnitude bandwidth of the resonant part and k_r/ω_c is the gain at $n\omega_0$. Note that $n_{\max}$ denotes the maximum order of grid current harmonics to be suppressed. The effects of k_r and ω_c have been broadly discussed in many studies. ω_c should be designed considering the slight variation of the actual grid frequency. In this study, ω_c is selected as 6 and k_r is 600. In the case of negligible grid impedance, the HR controller can realize a good performance, but some serious problems are encountered in the weak grid case [15]. In order to use a high n_{max} or k_r/ω_c for a high grid impedance, the phase compensated HR (PC-HR) is applied in the grid-connected application in these years [21], [22]. To extend the application of the proposed robust grid current control, the PC-HR controller is used. The PC-HR controller is:

$$G_{PC-HR}(s) = k_p + k_r \sum_{n=1,3,5,\ldots}^{n_{\max}} \frac{s\cos(\varphi_n) - n\omega_0 \sin(\varphi_n)}{s^2 + \omega_c s + (n\omega_0)^2} \tag{15}$$

where φ_n is the phase leading angel for each resonant part. The parameter selection can refer to [21] and [22].

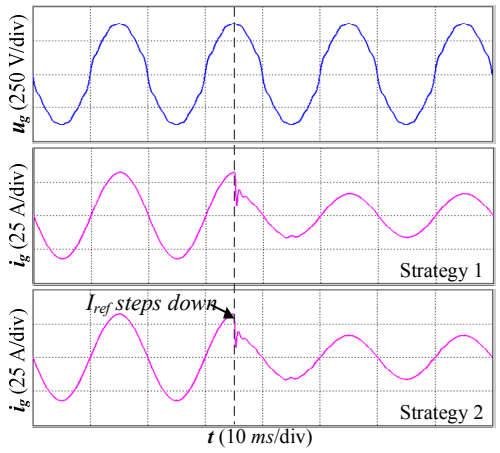

Fig. 8 Simulation waveforms with different strategies with Z_g=0

Then, simulation tests are carried out by using the above two current controllers.

Without Z_g, waveforms with different strategies are given in Fig. 8. The HR controller is adopted so that the THD of i_g is low. The grid current with Strategy 2 is almost the same as

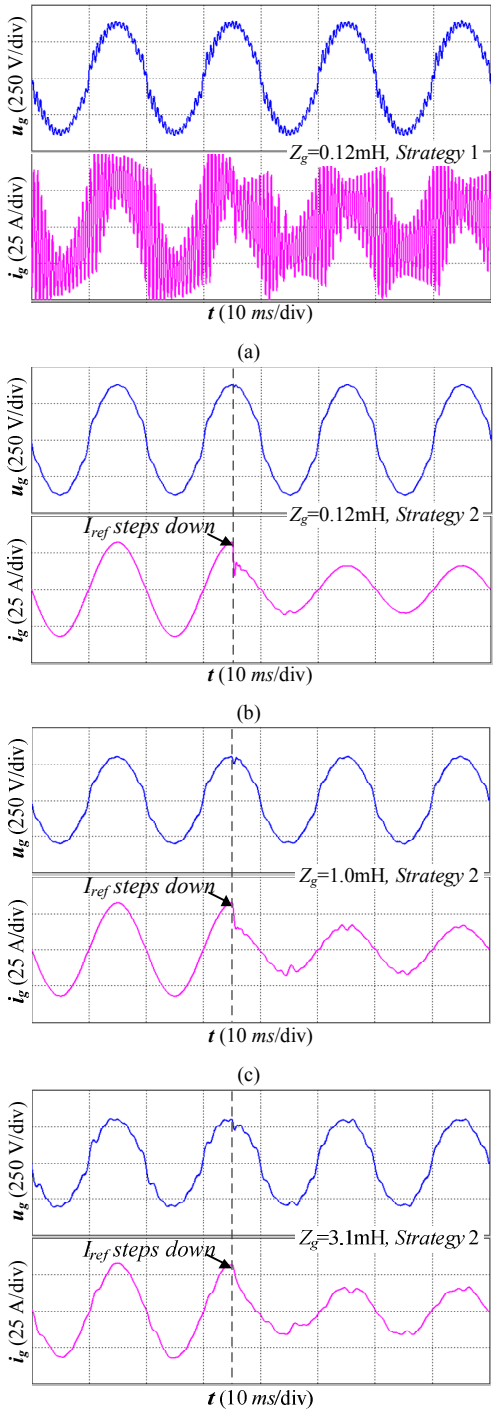

Fig. 9 Simulations with different strategies and Z_g, (a) Strategy 1 and Z_g=0.12mH, (b) Strategy 2 and Z_g=0.12mH, (c) Strategy 2 and Z_g=1.0mH, (d) Strategy 2 and Z_g=3.1mH

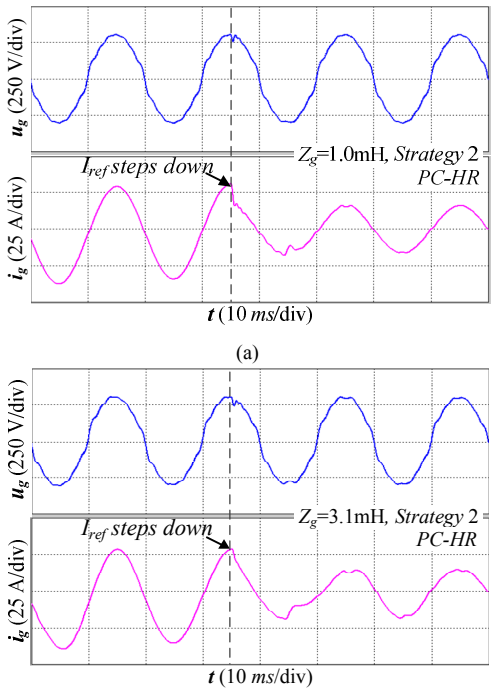

Fig. 10 Simulations with Strategy 2 using PC-HR in the case of (a) Z_g=1.0mH, and (b) Z_g=3.1mH

that with Strategy 1 (i.e., the same transient response), which verifies that the proposed phase shaping $G_{ps}(s)$ has a negligible impact on the dynamics below $f_{critical}$, as expected.

The performances are also tested in the presence of Z_g. The waveforms with different strategies are shown in Fig. 9. Many harmonics are aroused by Strategy 1, even when the grid impedance is small, i.e., only 0.12mH. However, with Strategy 2, the grid current is stable and slightly distorted. Even when the grid impedance increases up to 3.1mH, the inverter-grid system with Strategy 2 keeps stable. The instability caused by the typical GCFAD has been well solved.

Even though, it is emphasized that, in Figs. 9(c) and 9(d), once the current reference steps, some harmonics are aroused and those harmonics take a relatively long time to vanish. This phenomenon indicates a poor phase margin when using the HR controller in the weak grid case. By applying the PC-HR to improve the phases, the grid current harmonics during the transient response are more highly suppressed, as shown in Fig. 10, where the oscillations in the transient response are rapidly eliminated. The benefit of PC-HR has been verified again.

VI. Experiments

To further demonstrate the proposed grid current control, a single-phase inverter with the above *LCL* parameters is built for the experimental tests. A DSP TMS320F28035 is used for implementing the control. The amplitude of i_{ref} is set manually. The grid current waveforms in the weak grid case with the typical control in Fig. 2 and the proposed control in

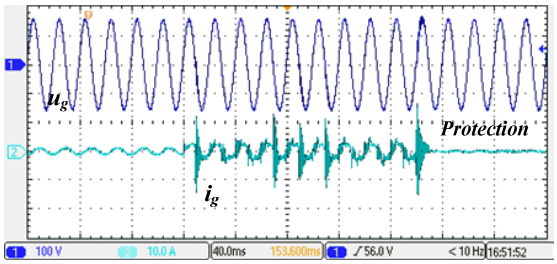

Fig. 11 Waveforms with the typical control with 0.2mH-grid impedance

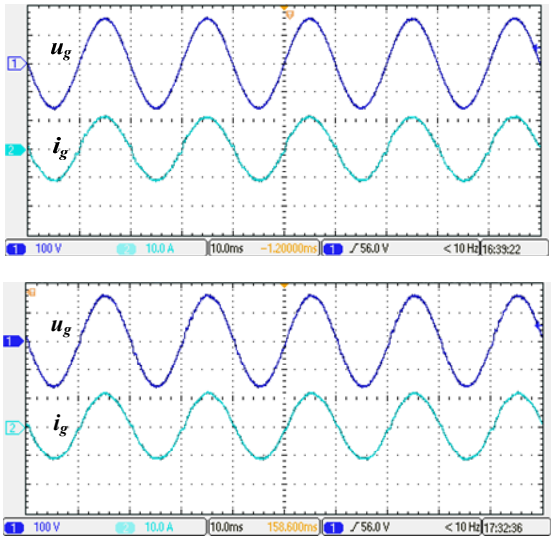

Fig. 12 Waveforms with the proposed control with (a) 0.2mH-grid impedance and (b) 2.5mH-grid impedance

Fig. 6 are given in Figs. 11 and 12. With the typical control, even if the grid impedance is very small, the system tends to be unstable and the protection is triggered during the start-up procedure. On the contrary, with the proposed grid current control, the harmonics appeared in Fig. 11 have been highly suppressed. Even if a large grid impedance is interfaced, the system with the proposed control owns a high robustness.

VII. Conclusions

The grid current feedback active damping only requires sampling the grid current and has a good application prospect in the grid-connected inverter for the cost reduction. But the grid impedance challenges the robustness because the phase of the inverter output impedance at a specific frequency can be close to or below −90° depending on the proportional gain of current controller. As a result, the contradiction between the high bandwidth and high robustness is yielded. Therefore, this study proposes adding a proper phase shaping compensator to improve the robustness. The selection of controller parameters has been discussed and simulation and experimental results have been provided. It has been proved that the phase shaping compensator improves the stability in the weak grid case.

ACKNOWLEDGMENT

This work was supported by the National Natural Science Foundation of China (No. 51477077).

REFERENCES

[1] X. Guo, W. Liu and Z. Lu, "Flexible power regulation and current-limited control of the grid-connected inverter under unbalanced grid voltage faults," *IEEE Trans. Ind. Electron.*, Vol. 64, No. 9, pp. 7425-7432, Sept. 2017.

[2] J. Xu and S. Xie, "*LCL*-resonance damping strategies for grid-connected inverters with LCL filters: a comprehensive review", *J. Mod. Power Syst. Clean Energy*, 2017, doi: 10.1007/s40565-017-0319-7.

[3] R.N. Beres, X. Wang, M. Liserre, and F. Blaabjerg, "A review of passive power filters for three-phase grid-connected voltage-source converters," *IEEE J. Emerg. Sel. Top. Power Electron.*, vol. 4, no. 1, pp. 54–69, Mar. 2016.

[4] J. Wang, J. D. Yan, L. Jiang and J. Zou, "Delay-dependent stability of single-loop controlled grid-connected inverters with *LCL* filters," *IEEE Trans. Power Electron*., vol. 31, no. 1, pp. 743-757, Jan. 2016.

[5] J. Xu, S. Xie, L. Huang and L. Ji, "Design of *LCL*-filter considering the control impact for grid-connected inverter with one current feedback only," *IET Power Electron.*, vol. 10, no. 11, pp. 1324-1332, Sep. 2017.

[6] J. Dannehl, M. Liserre and F. W. Fuchs, "Filter-based active damping of voltage source converters with *LCL* filter," *IEEE Trans. Ind. Electron.*, vol. 58, no. 8, pp. 3623–3633, Aug. 2011.

[7] Y. Liu, W. Wu, Y. He, Z. Lin, F. Blaabjerg and H. S. H. Chung, "An efficient and robust hybrid damper for *LCL*- or *LLCL*-based grid-tied inverter with strong grid-side harmonic voltage effect rejection," *IEEE Trans. Ind. Electron.*, vol. 63, no. 2, pp. 926-936, Feb. 2016.

[8] J. Xu, S. Xie, and B. Zhang, "Current harmonics rejection and improvement of inverter-side current control for the LCL filters in grid-connected applications," *Journal of Power Electronics*, vol. 17, no. 6, pp. 1672-1682, Nov. 2017.

[9] W. Yao, Y. Yang, X. Zhang, F. Blaabjerg, and P. C. Loh, "Design and analysis of robust active damping for *LCL* filters using digital notch filters," *IEEE Trans. Power Electron.*, vol. 32, no. 3, pp.2360-2375, Mar. 2017.

[10] J. Xu, S. Xie, and T. Tang, "Active damping-based control for grid-connected *LCL*-filtered inverter with injected grid current feedback only," *IEEE Trans. Ind. Electron.,* vol. 61, no. 9, pp.4746-4758, Sept. 2014.

[11] M. Hanif, V. Khadkikar, W. Xiao and J. L. Kirtley, "Two degrees of freedom active damping technique for *LCL* filter-based grid connected PV systems," *IEEE Trans. Ind. Electron.*, vol. 61, no. 6, pp. 2795-2803, June 2014.

[12] L. Zhou, Y. Chen, A. Luo, J. M. Guerrero, X. Zhou, Z. Chen and W. Wu , "Robust two degrees-of-freedom single-current control strategy for *LCL*-type grid-connected DG system under grid-frequency fluctuation and grid-impedance variation," *IET Power Electron.*, vol. 9, no. 14, pp. 2682-2691, Nov. 2016.

[13] X. Wang, F. Blaabjerg and P. C. Loh, "Grid-current-feedback active damping for *LCL* resonance in grid-connected voltage-source converters," *IEEE Trans. Power Electron.*, vol. 31, no. 1, pp. 213-223, Jan. 2016.

[14] J. Sun, "Impedance-based stability criterion for grid-connected inverters," *IEEE Trans. Power Electron.,* vol. 26, no. 11, pp. 3075-3078, Nov. 2011.

[15] J. Xu, S. Xie, and T. Tang, "Evaluations of current control in weak grid case for grid-connected *LCL*-filtered inverter," *IET Power Electron.,* vol. 6, no. 2, pp. 227-234, Feb. 2013.

[16] M. Cespedes and J. Sun, "Impedance modeling and analysis of grid-connected voltage-source converters," *IEEE Trans. Power Electron.*, vol. 29, no. 3, pp. 1254–1261, Mar. 2014.

[17] D. Yang, X. Ruan and H. Wu, "Impedance shaping of the grid-connected inverter with *LCL* filter to improve its adaptability to the weak grid condition," *IEEE Trans. Power Electron.*, vol. 29, no. 11, pp. 5795-5805, Nov. 2014.

[18] L. Harnefors, X. Wang, A. G. Yepes, and F. Blaabjerg, "Passivity-based stability assessment of grid-connected VSCs—An overview," *IEEE J. Emerg. Sel. Top. Power Electron.*, vol. 4, no. 1, pp. 116-125, Mar. 2016.

[19] X. Chen, Y. Zhang, S. Wang, J. Chen and C. Gong, "Impedance-phased dynamic control method for grid-connected inverters in a weak grid," *IEEE Trans. Power Electron.*, vol. 32, no. 1, pp. 274-283, Jan. 2017.

[20] J. Xu, S. Xie, Q. Qian, and B. Zhang, "Adaptive feedforward algorithm without grid impedance estimation for inverters to suppress grid current instabilities and harmonics due to grid impedance and grid voltage distortion," *IEEE Trans. Ind. Electron*., vol. 64, no. 9, pp. 7574-7586, Sept. 2017.

[21] Q. Qian, S. Xie, L. Huang, J. Xu, Z. Zhang, and B. Zhang, "Harmonic suppression and stability enhancement for parallel multiple grid-connected inverters based on passive inverter output impedance," *IEEE Trans. Ind. Electron*., vol. 64, no. 9, pp. 7587-7598, Sept. 2017.

[22] X. Wang, F. Blaabjerg and P. C. Loh, "Virtual RC damping of *LCL*-filtered voltage source converters with extended selective harmonic compensation," *IEEE Trans. Power Electron*., vol. 30, no. 9, pp. 4726-4737, Sept. 2015.